This article has been accepted for publication in a future issue of this journal, but has not been fully edited. Content may change prior to final publication. Citation information: DOI 10.1109/TPWRD.2018.2881221, IEEE Transactions on Power Delivery

Voltages and AC Corrosion on Metallic Tubes in Umbilical Cables Caused by Magnetic Induction From Power Cable Charging Currents

Bjørn Gustavsen, *Fellow, IEEE*, Martin Høyer-Hansen, Marius Hatlo, and Steinar Midttveit

.

***Abstract*—Offshore umbilical cables often include both power cables and elements such as metallic tubes and signal cables. It was concluded from a recent failure of stainless tubes that AC corrosion was the failure cause. This paper describes how AC corrosion can lead to tube failure if a puncture exists in the insulating tube coating. The variation in power cable charging currents along the umbilical cable causes a non-zero voltage to exist on the tubes, even though they are grounded at both ends. If the current density associated with the puncture current is sufficiently high, AC corrosion will result. The current density is calculated as function of cable length and VSD operating frequency, for three alternative power cable designs. Comparison with measured corrosion rates shows that AC corrosion can corrode a hole in the tube in weeks or months, depending on the cable design and length, and on the electrical operating conditions. Analytical expressions and numerical procedures are presented which can be used to determine if a given umbilical cable installation involves risk of AC corrosion. It is also shown that substantial heating effects in the puncture area can result in case of excessive harmonics in the supply voltage.**

***Index Terms*— Umbilical cable, power cable, charging current, AC corrosion, tubes.**

I. Introduction

POWER umbilical cables are widely used in offshore oil and gas applications for providing electric power to subsea installations, e.g. subsea pumps and compressors. In addition to supplying electrical power at medium voltage, they usually include other elements such as signal cables, fiber optic cables, and tubes which carry chemical fluids. The length of such cables can reach up to a few tens of kilometers. It follows that the reliability of the umbilical cables is essential for the economy of the installation.

There have recently been some failures to power cables [1] and power umbilicals, caused by electromagnetic interference between power phases and embedded metallic tubes. The interference has caused severe damage to the power phases with resulting insulation failure, as well as leakage from steel tubes in the case of umbilical cables. In this paper the main focus is on power umbilicals, where the tubes are typically super-duplex (SD) steel with an insulating outer sheath. If the tube sheathing gets damaged such that the metallic tube is exposed to seawater (ground) in a confined area, the electromagnetic interference may cause high local current density at the unintended grounding point, with corresponding AC corrosion and heat development. AC corrosion is a phenomenon where an AC current flows from a metallic surface into an electrolyte. The drift of metallic ions can then cause local corrosion (pitting) if the current density is sufficiently high. The actual corrosion rate depends on the material type, the electrolyte involved, on the current density, and other parameters [1],[2]. Additionally, if the induced voltage is sufficiently high, local heating effects and arcing can potentially take place in the area where the tube is exposed to seawater/ground, causing severe damage to the surrounding elements inside the umbilical/cable.

The same phenomenon of induced voltage and AC corrosion can occur also for buried pipelines sharing a common right-of-way with overhead electric power lines [2], [3]. As stated in [2], “the largest induced voltage levels occur at locations along the pipeline where the power line electric field changes value due to some form of electrical or physical discontinuity”, and such discontinuity is typically a physical change in either the power line geometry (transposition) or change in distance between pipeline and the power line. As the power phases and geometry is fixed for a power umbilical, the normal procedure is to ground the SD tubes at both ends and then assume that the voltage along these metallic parts is zero.

In this work we show that in the case of umbilical cables of substantial length, a non-negligible voltage will develop on insulated metallic tubes and armors even when they are solidly grounded at both ends. We show that the cause for this voltage development is the charging currents in the power cables which cause an uneven magnetic induction to the tubes/armors along the cable. A small puncture or exposed area can then lead to high current density from the tube metal into the umbilical annulus which is flooded with sea water, thereby starting the corrosion process. The analysis is performed based on a representative umbilical cable with three alternative power cable designs that differ in terms of metallic screens and semiconductive outer layers. Analytical formulae are

Manuscript received March XXX, 2018.

B. Gustavsen and M. Høyer-Hansen are with SINTEF Energy Research, NO 7465 Trondheim, Norway (bjorn.gustavsen@sintef.no, martin.hoyer-hansen@sintef.no).

M. Hatlo is with Nexans Norway AS, NO-1751 Halden, Norway (marius.hatlo@nexans.no).

S. Midttveit is with Statoil ASA, NO-5171 Bergen, Norway (stmid@statoil.com)

This article has been accepted for publication in a future issue of this journal, but has not been fully edited. Content may change prior to final publication. Citation information: DOI 10.1109/TPWRD.2018.2881221, IEEE Transactions on Power Delivery

derived for each design developed which permit to calculate the voltage on the SD tubes at the operating frequency. A complementary procedure is presented which allows to calculate the voltage in the presence of higher frequencies, including harmonics. Using the numerical model in combination with a model of the coating puncture, the current density is calculated for a 15 km umbilical with power cables supplied at 11 kV. The calculated current density is used for estimating the time to puncture of the SD tube wall by comparison with measurements of the corrosion rate for a representative SD tube material with alternative current densities and frequencies.

Additionally, we analyze the possibility of excessive tube voltages resulting from resonance effects in the cable if the cable is fed from a source with substantial harmonic components. The possibility of local heating problems in a tube puncture is evaluated.

II. Power Cable Designs

In the analysis we consider three alternative designs of the single-core (SC) power cables that are used in subsea umbilical cables. In all cases the cable consists of a conductor, inner semiconductive screen, insulation and outer semiconductive screen. The external part of the cable can differ as follows.

1) Cable without metallic screen (screenless). A semiconductive layer is used as jacket for the cable, without any metallic screen. The SC cables are brought in contact with each other and the external armor, directly or via semiconductive fillers, thereby providing a conductive path for the charging currents. This design benefits from reduced losses since there are no screen currents flowing.
2) Cable with metallic screen and semiconductive jacket. A metallic screen is covered with a semiconductive jacket. The cables in the umbilical cable are brought in contact with each other and the external armor, directly or via semiconductive fillers. Charging currents will cancel through the semiconducting sheath, and screen voltage will be zero.
3) Cable with metallic screen and insulating jacket. A metallic screen is covered with an insulating jacket and grounded at both ends. The metallic screen provides the return path for the charging currents. This design has a range/voltage limit since the screen voltage increases with increasing cable length and operating voltage.

III. Induced Voltages at Fundamental Frequency

The following subsections III.A, III.B and III.C derive analytical expressions for calculating the voltage buildup on metallic tubes for the three cable designs in Section II. The generalization to three-phase systems is shown in Section III.D. It is assumed that the frequency is so low that there are no resonance effects in the cables.

A. Cable Without Metallic Screen (Screenless)

To understand the nature of the voltage build-up, we consider a system of two parallel conductors. The first conductor (line 1) represents the power conductor while the second conductor (line 2) represents an insulated tube. For an infinitesimal section length along the cable, we have the per-unit-length (PUL) relation between voltage drops and currents,

$$-\frac{d}{dx}\begin{bmatrix} V_1 \\ V_2 \end{bmatrix} = \begin{bmatrix} Z_{11} & Z_{12} \\ Z_{21} & Z_{22} \end{bmatrix} \cdot \begin{bmatrix} I_1 \\ I_2 \end{bmatrix} \tag{1}$$

$$-\frac{d}{dx}\begin{bmatrix} I_1 \\ I_2 \end{bmatrix} = j\omega \begin{bmatrix} C_{10} & 0 \\ 0 & C_{20} \end{bmatrix} \cdot \begin{bmatrix} V_1 \\ V_2 \end{bmatrix} \tag{2}$$

Consider that the first line is energized with a sinusoidal current at the sending end and loaded at the receiving end as shown in Fig. 1. The second line is grounded at both ends. If one ignores the charging currents, the current is constant along line 1 and so the induced voltage along line 2 is also constant. As a result, there will at any position x be a current induced in line 2 whose voltage drop ($Z_{22}I_2$) exactly balances the induced voltage ($Z_{21}I_1$) in the line. Therefore, the voltage is exactly zero at any position along line 2.

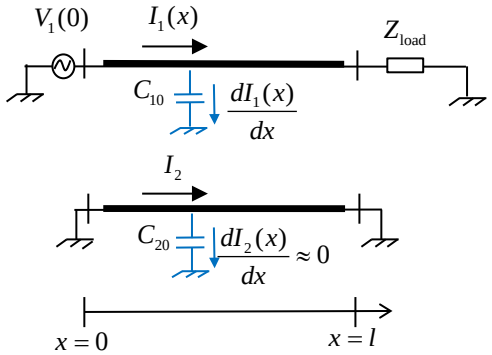

Fig. 1. Induced current in line 2 from current in line 1.

When charging currents are included, the induced voltage will vary along line 2 since the charging is not constant along line 1. Therefore, the induced voltage in line 2 cannot be perfectly balanced by voltage drop caused by the induced current in that line. To calculate the induced voltage, we will make three simplifications: 1) The voltage along line 1 is constant, 2) the charging currents associated with the voltage on line 2 is negligible, and 3) there is no direct capacitive coupling between the lines. To simplify the analysis we assume to start with that the load impedance is infinite so that all charging current is fed from the source end, and we also ignore the system losses.

The charging current along line 1 is

$$I_1(x) = j\omega C_{10}(l-x)V_1 \tag{3}$$

Inserting (3) into the second equation in (1) and integrating from 0 to x gives for the voltage on line 2 at position x,

$$V_2(x) = -j\omega Z_{21}C_{10}V_1\left(lx - \frac{1}{2}x^2\right) - Z_{22}I_2x \tag{4}$$

Evaluating (4) at $x=l$ and imposing the condition $V_2(l) = 0$ gives for the current

This article has been accepted for publication in a future issue of this journal, but has not been fully edited. Content may change prior to final publication. Citation information: DOI 10.1109/TPWRD.2018.2881221, IEEE Transactions on Power Delivery

$$I_2 = \frac{-j\omega Z_{21} C_{10} V_1 l}{2 Z_{22}} \tag{5}$$

Inserting the currents (3) and (5) into the second equation of (1) and imposing the condition $dV_2(x)/dx=0$ defines the point where $V_2(x)$ is maximum, which is found to be at the line mid-point $x^* = l/2$. At this position we get, using (4) with I_2 from (5), the maximum voltage along line 2 (tube),

$$\hat{V}_2 = V_2(\frac{l}{2}) = \frac{j\omega Z_{21} C_{10} l^2}{8} V_1 \approx \frac{-\omega^2 L_{21} C_{10} l^2}{8} V_1 \tag{6}$$

Equation (6) shows that the maximum tube voltage is proportional to L_{21} and C_{10}, and to the square of the operating frequency and the line length.

In the derivation we assumed that the charging current was fed from the sending end of line 1 (power cable). The solution (6) is however valid for any distribution of the charging current between the two line ends. This result follows because the (linear) distribution of the charging current is changed only by an offset.

B. Cable With Metallic Screen and Semiconductive Jacket

In some umbilical designs, the insulating jacket outside the metallic sheath is replaced with a semiconductive layer. The design is usually such that semiconductive filler elements are included is the umbilical so that there exists a semiconductive path between all cable screens. That way, the buildup of voltages along the metallic screens is avoided as the induced voltage will discharge in the radial direction.

The induced tube voltage can be analyzed using the same formulae as in Section III.A (cable without metallic screen) but with a different value of L_{21}. The value of L_{21} to be used results by eliminating the metallic screens from the PUL series impedance matrix **Z** by setting $dV/dx = 0$ on the metallic screens.

C. Cable With Metallic Screen And Insulating Jacket

We now consider that the power cable is fitted with a metallic screen and an insulating jacket. The PUL parameters becomes as in (7) and (8) where conductor, screen and tube are numbered 1, 2 and 3, respectively. C_{12}, C_{20} and C_{30} are respectively the partial capacitances between conductor and screen, between screen and water, and between tube and water.

$$-\frac{d}{dx}\begin{bmatrix} V_1 \\ V_2 \\ V_3 \end{bmatrix} = \begin{bmatrix} Z_{11} & Z_{12} & Z_{13} \\ Z_{21} & Z_{22} & Z_{23} \\ Z_{31} & Z_{32} & Z_{33} \end{bmatrix} \cdot \begin{bmatrix} I_1 \\ I_2 \\ I_3 \end{bmatrix} \tag{7}$$

$$-\frac{d}{dx}\begin{bmatrix} I_1 \\ I_2 \\ I_3 \end{bmatrix} = j\omega \begin{bmatrix} C_{12} & -C_{12} & 0 \\ -C_{12} & C_{20} & 0 \\ 0 & 0 & C_{30} \end{bmatrix} \cdot \begin{bmatrix} V_1 \\ V_2 \\ V_3 \end{bmatrix} \tag{8}$$

We consider the induction from a single-core cable whose screen is grounded at both ends, see Fig. 2. With the assumption that the screen voltage is much lower than the conductor voltage, the charging current flowing from the conductor to the screen is constant along the cable, given as

$$\frac{dI_1(x)}{dx} = j\omega C_{12}(V_1 - V_2) \approx j\omega C_{12} V_1 \tag{9}$$

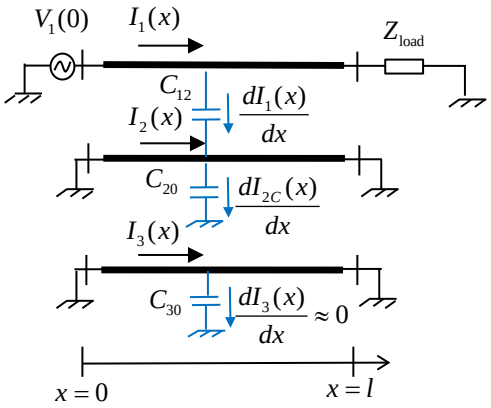

Fig. 2. Induced currents from current in line 1.

This capacitive charging current divides evenly between the two screen ends, giving a linear current distribution along the screen,

$$I_2(x) = -j\omega C_{12} V_1 (\frac{l}{2} - x),\ x \in [0, \frac{l}{2}) \tag{10a}$$

$$I_2(x) = j\omega C_{12} V_1 (\frac{l}{2} - x),\ x \in (\frac{l}{2}, l] \tag{10b}$$

$$I_2(x) = 0,\ x = \frac{l}{2} \tag{10c}$$

The voltage along the screen is dominated by the resistive voltage drop along the screen that is caused by the capacitively induced screen current. With a PUL screen resistance R_S, the screen voltage in the left half of the cable is

$$V_2(x) = -\int_0^x R_S I_2(x) dx = -\frac{j\omega C_{12} R_S V_1}{2} x(x-l),\ x \in [0, \frac{l}{2}) \tag{11}$$

The voltage on the screen leads to a secondary charging current component from the screen to ground. The change in charging current per unit length is

$$-\frac{d}{dx} I_{2C}(x) = j\omega C_{20} V_2(x) = \frac{\omega^2 C_{12} C_{20} R_S V_1}{2} x(x-l) \tag{12}$$

The accumulated charging current along the screen is

$$I_{2C}(x) = -\int_x^{l/2} \frac{d}{dx} I_{2C}(x) dx = -\int_x^{l/2} \frac{\omega^2 C_{12} C_{20} R_S V_1}{2} x(x-l) dx \tag{13}$$

Carrying out the integration of (13) gives

$$I_{2C}(x) = -\frac{\omega^2 C_{12} C_{20} R_S V_1}{2} (\frac{1}{2} x^2 l - \frac{1}{3} x^3 - \frac{1}{12} l^3) \tag{14}$$

The induced voltage on the tube from $I_{2C}(x)$ is obtained from

$$-\frac{dV_3(x)}{dx} = Z_{32} I_{2C}(x) + Z_{33} I_3,\ x \in [0, \frac{l}{2}) \tag{15}$$

This article has been accepted for publication in a future issue of this journal, but has not been fully edited. Content may change prior to final publication. Citation information: DOI 10.1109/TPWRD.2018.2881221, IEEE Transactions on Power Delivery

Equation (15) is zero at $x=l/2$ which gives $I_3=0$, as could be expected from symmetry. Integrating (15) from 0 to x gives the tube voltage as

$$V_3(x) = Z_{32}\frac{\omega^2 C_{12}C_{20}R_S V_1}{2}\left(\frac{1}{12}x^4 - \frac{1}{6}x^3 l + \frac{1}{12}l^3 x\right) \quad (16)$$

The voltage is maximum when $x=l/2$,

$$V_3\left(\frac{l}{2}\right) = \omega^2 Z_{32}C_{12}C_{20}R_S\, l^4\,\frac{5}{384}V_1 \quad (17)$$

With the assumption $Z_{32}\approx j\omega L_{32}$, (17) simplifies to

$$\hat{V}_3 = V_3\left(\frac{l}{2}\right) = -j\omega^3 L_{32}C_{12}C_{20}R_S\, l^4\,\frac{5}{384}V_1 \quad (18)$$

It is observed from (18) that the tube voltage is proportional to the third power of frequency and the fourth power of cable length. It is further proportional to the screen resistance and to the core-screen and screen-earth capacitances.

D. Three-Phase Circuits

In the case of induction from a three-phase power circuit with line voltage $\sqrt{3}V_1$, the tube voltage inductions (6) and (17) are obtained as the vector sum of the induction from the three power cables. Let the the power cables be denoted *a*, *b*, *c*. In the screenless and screened case we respectively get

$$V_2\left(\frac{l}{2}\right) = j\frac{\omega C_{10} l^2}{8}\left(Z_{21,a} + h^2 Z_{21,b} + hZ_{21,c}\right)V_1 \quad (19)$$

$$V_3\left(\frac{l}{2}\right) = \omega^2 C_{12}C_{20}R_S\, l^4\left(Z_{32,a} + h^2 Z_{32,b} + hZ_{32,c}\right)\frac{5}{384}V_1 \quad (20)$$

where $h = e^{j2\pi/3}$.

IV. Induced Voltages at Harmonic Frequencies

A. Frequency Domain Calculations

The analytical expressions (19) and (20) are useful for estimating the tube voltages during normal operation at 50/60 Hz or at variable speed drive (VSD) frequencies. When analyzing situations with higher frequency components, e.g. harmonic emissions from a VSD, the voltage along the phase conductors can no longer be assumed to be constant due to resonance effects in the cables. In that case, the calculations can be performed in the frequency domain using nodal analysis whereby the system of conductors is represented by a cascade of exact PI-equivalents. Such approach also allows to handle any number of conductors, the (pump) loading effect, and to study the effect of punctures in the tube coating which is necessary in studies of AC corrosion.

For an *n*-conductor homogenous line, we have in the frequency domain,

$$-\frac{d\mathbf{v}(\omega)}{dx} = \mathbf{Z}(\omega)\mathbf{i}(\omega) \quad (21)$$

$$-\frac{d\mathbf{i}(\omega)}{dx} = \mathbf{Y}(\omega)\mathbf{v}(\omega) \quad (22)$$

where **v** and **i** are vectors of length *n*, and **Z** and **Y** are matrices of dimension $n\times n$,

$$\mathbf{Z}(\omega) = \mathbf{R}(\omega) + j\omega\mathbf{L}(\omega) \quad (23)$$

$$\mathbf{Y}(\omega) = \mathbf{G}(\omega) + j\omega\mathbf{C}(\omega) \quad (24)$$

In the case of cables with XLPE and PE insulation, **G** is practically zero and **C** is independent of frequency. The cable of length l is divided into N segments which are modeled by an exact PI-equivalent. The nodal admittance stamp associated with the exact PI-equivalent is given by (25) and (26) [5],

$$\mathbf{Y}_n = \begin{bmatrix} \mathbf{A} & \mathbf{B} \\ \mathbf{B} & \mathbf{A} \end{bmatrix} \quad (25)$$

$$\mathbf{A} = \mathbf{Z}^{-1}\mathbf{S}\hat{\mathbf{A}}\mathbf{S}^{-1},\ \mathbf{B} = \mathbf{Z}^{-1}\mathbf{S}\hat{\mathbf{B}}\mathbf{S}^{-1} \quad (26)$$

$\hat{\mathbf{A}}$ and $\hat{\mathbf{B}}$ are diagonal matrices whose (diagonal) elements are given by (27) and (28),

$$A_m = \frac{\sqrt{\Lambda_m}(1+\xi_m^2)}{(1-\xi_m^2)},\ B_m = \frac{-2\sqrt{\Lambda_m}\,\xi_m}{(1-\xi_m^2)} \quad (27)$$

$$\xi_m = e^{-\sqrt{\Lambda_m}\,l_{\text{seg}}} \quad (28)$$

Λ_m and **S** are the eigenvalues and eigenvector matrix associated with the matrix product **ZY**, i.e.,

$$\mathbf{ZY} = \mathbf{S}\boldsymbol{\Lambda}\mathbf{S}^{-1} \quad (29)$$

Using frequency domain nodal analysis, the PI-sections are cascaded to give a model of the complete cable. It is to be observed that the calculated result in the observation points does not depend on the number of segments since exact PI-elements are used.

B. Time Domain Calculations

In the case of tube voltages arising from VSD harmonic emission, it is convenient to perform the calculations directly in the time domain. There are to main alternatives.

1) If voltage time domain measurements have been performed at the umbilical topside end, one may apply these voltages as ideal voltage sources to a rational function type model (30) that represents the voltage transfer function from topside cable terminals to selected point(s) along the tubes. The time domain voltages at these points can then be calculated as function of time via recursive convolution (31). The transfer functions are calculated in the frequency domain using nodal analysis and subjected to fitting [6] by the rational model, with the cable load included in the frequency domain calculations. The application of this approach is shown in Section X.

$$H_{1\times 3}(\omega) = R_{1\times 3,0} + \sum_i \frac{R_{1\times 3,i}}{j\omega - a_i} \quad (30)$$

$$v_{tube}(t) = h_{1\times 3}(t) * [v_a(t) \quad v_b(t) \quad v_c(t)]^T \quad (31)$$

This article has been accepted for publication in a future issue of this journal, but has not been fully edited. Content may change prior to final publication. Citation information: DOI 10.1109/TPWRD.2018.2881221, IEEE Transactions on Power Delivery

2) If measurements are not available, one may apply a time domain simulation model of the complete system for obtaining the topside voltages. In the simulation one may represent the cable and its loading impedance by a rational function-based terminal equivalent with a parallel current source for representing the counter emf of a motor load.

V. AC Corrosion Phenomenon

A. Phenomenon

The presence of an induced voltage on coated (insulated) tubes may lead to a phenomenon known as AC corrosion, if there is a puncture in the coating. The voltage causes an alternating current to cross the metal/electrolyte interface, in this case from super-duplex (SD) steel to the sea water that is flooding the umbilical. The governing AC corrosion model [7] explains that the steel surface is oxidized during the positive (anodic) half-wave of the AC cycle by the faradaic reaction

$$Fe \rightarrow Fe^{2+} + 2e^{-} \tag{32}$$

This process leads to the formation of a passive film on the surface during the positive half-cycle which is not reversed during the negative (cathodic) half-cycle. Instead, the passive film is converted into a porous layer of rust.

B. Impedance of Puncture Channel

The introduction of a puncture in the SD tube coating gives rise to a current I_{leak} that will flow through the puncture, depending on the driving voltage V and the impedance of the path Z_{path}. In electrochemistry, an electrode in an electrolyte is represented by a Randles equivalent electrical circuit, as shown in Fig. 3 [8]. The circuit consists of an electrolyte resistance R_{s} in series with a double layer capacitance C_{dl} connected in parallel with a faradaic reaction resistance R_{ct}. A Warburg element Z_{w} is introduced in series with R_{ct}, representing the diffusion (or mass transfer) behavior of the reaction agents.

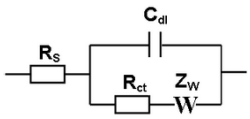

Fig. 3. Randles equivalent electrical circuit for metal-electrolyte interface.

Thus, the path impedance is given as

$$Z_{\text{path}} = R_{\text{s}} + Z_{\text{dl}} \tag{33}$$

where Z_{dl} is the total impedance of the metal-electrolyte interface elements.

In the case of a coating defect, R_s is assumed to be comprised of two parts; i) the resistance R_{channel} through the coating defect void, and ii) the spread resistance R_{spread} outside the coating to remote ground. For an umbilical with insulating outer sheath, remote ground is located at each end of the umbilical, and R_{s} includes the total impedance towards the ends. If a homogeneous circular coating defect of cross-section area A is considered, the channel resistance is

$$R_{\text{channel}} = \frac{t}{\sigma A} \tag{34}$$

where t is the thickness of the coating and σ is the conductivity in the void.

Including the resistance in the electrolyte towards remote earth, the formula for the full path impedance is similar to the resistance of a circular anode of area A in series with the channel resistance and the double layer impedance can be approximated as

$$Z_{\text{path}} = \frac{t}{\sigma A} + \frac{1}{2.6\sigma\sqrt{A}} + Z_{\text{dl}} \tag{35}$$

The double layer impedance Z_{dl} is a barrier impeding charge transfer. It varies with material type, cathodic protection level, frequency, voltage etc. As a conservative approach, both double layer impedance and umbilical environment will be ignored in the following analyses

C. Current Density And Corrosion Rate

The rate of AC corrosion is related with the AC current density J of the current that leaves the metal surface

$$J = \frac{I_{\text{leak}}}{A} \tag{36}$$

as well as other parameters, including steel quality, temperature, frequency and cathodic protection level. General guidelines on AC corrosion given in standards may provide an indication of the AC corrosion risk [9] which states that there is no risk of AC corrosion for current density levels below 30 A/m^2 when the power frequency is between 16.7 Hz and 60 Hz. The rate of corrosion increases with increasing current densities [9], [10].

VI. Measurement of AC Corrosion Rate

Table I shows measurement results of the corrosion rate for an SD tube material. The measurements were performed on circular test samples with 5 mm radius as described in British Standard 15280. The measurements were done at atmospheric pressures and with standard sea water solution. Each number represents the measured loss of material (weight) which has been converted into an equivalent thickness per time unit [mm/year]. The numbers in parenthesis denote the number of days needed to corrode away a tube with 2 mm wall thickness. It is observed that at 50 Hz, a current density of J=250 A/m^2 gives a corrosion rate of 0.25 mm/year which increases to 6.3 mm/year with J=1000 A/m^2. In the latter case, puncture is expected within 116 days. It is further seen that the corrosion rate is reduced with increasing frequency (at constant current density). AC corrosion also occurs at higher frequencies, however at a higher current density.

When inspecting the samples it was found that the corrosion is not entirely uniform over the sample surface as some local pitting takes place. Therefore, it is likely that the time to puncture will be lower than indicated in Table I.

Table I. Corrosion rate [mm/year] ([days to failure])

This article has been accepted for publication in a future issue of this journal, but has not been fully edited. Content may change prior to final publication. Citation information: DOI 10.1109/TPWRD.2018.2881221, IEEE Transactions on Power Delivery

	100 A/m^2	250 A/m^2	1000 A/m^2
50 Hz	<0.01	0.25 (2920)	6.3 (116)
100 Hz		0.03 (24000)	1.3 (561)
200 Hz		<0.01	0.3 (2400)

VII. Umbilical Cable System

A. Geometry

As an example we consider an umbilical cable of 15 km length which has one three-phase power circuit, five tubular flow lines (super-duplex steel coated with PE), and one fiber optic element. The elements are placed around one insulating tube, and inside a two-layer steel armoring, see Fig. 4. The power circuit is typically used for supplying a pump or compressor motor as part of a variable speed drive (VSD). Information about the various elements are given in Tables II-IV. The steel armoring has an outer diameter of 145 mm with 70 and 80 wires in the inner and outer layer, respectively. The assumed steel wire conductivity and permeability are $5{\cdot}10^6$ S/m and 100, respectively. The fiber optic (FO) element has an inner stainless steel tube and a steel wire armoring.

The induced voltage om the SD tubes will be calculated for the three SC cable designs described in Section II. The variants are achieved by replacing either the insulating jacket, or both the metallic screen and insulating jacket, with a semiconductive jacket. The position and diameter of each SC cable in Fig. 3 remains unchanged.

B. PUL Parameters

The umbilical cable is submerged and flooded with sea water with conductivity 3.3 S/m. The conductors are associated with the phase numbering shown in Fig. 3 while the steel armoring is assumed to be on ground potential. The impedance matrix of this 12×12 system is calculated at any frequency using the MoM-SO method [11] which includes both skin and proximity effect while enforcing that the net current is the same in all wires in each armor layer [12]. The capacitance calculations assume that the surface of all elements is on ground potential as the umbilical is flooded. The contributions to the capacitance matrix can then be calculated for each element inside the umbilical individually. Standard analytical expressions are used for the power cables and tubes while FEM computations are used for the fiber optic element.

C. Electrical System

The power cables are fed from a 11 kV (line-line) three-phase voltage source at 50 Hz. The cable screens, tubes, and the FO armoring are grounded at both cable ends as shown in Fig. 5.

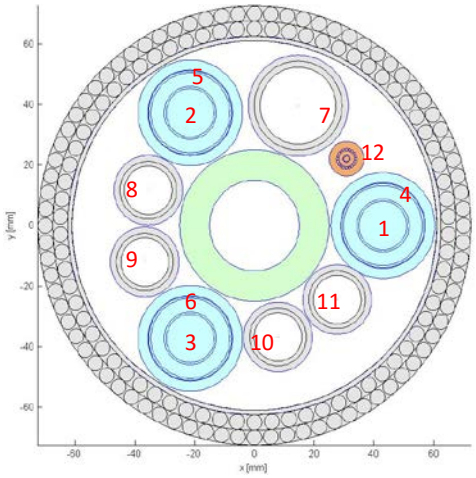

Fig. 4. Armored three-core cable with conductor numbering.

Table II. Power cables.

Item	OD [mm]	t [mm]	Rdc [Ω/km]	σ [S/m]	ε_r
Conductor	16		0.099		
Inner semicon		0.7			
Insulation		4.5			2.3
Outer semicon		0.7			
Sheath		0.15		$58{\cdot}10^6$	
Jacket		3.3			2.3

Table III. SD tubes, Type A (1 of).

Item	OD [mm]	t [mm]	σ [S/m]	μ_r	ε_r
SD tube	29.4	2	$1.3{\cdot}10^6$	20	
Jacket		2			2.3

Table IV. SD tubes, Type B (four of).

Item	OD [mm]	t [mm]	σ [S/m]	μ_r	ε_r
SD tube	19	1.519	$1.3{\cdot}10^6$	20	
Jacket		2			2.3

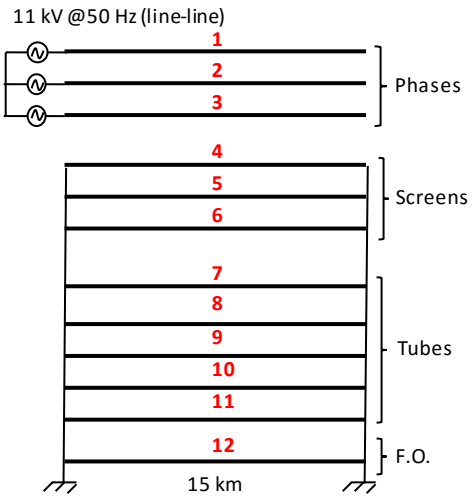

Fig. 5. Application of voltages and groundings. 15 km length.

VIII. Tube Voltages at Operating Frequencies

Fig. 6 shows the induced voltage along the tubes and the fiber optic element with operation at 11 kV and 50 Hz, for the three alternative designs, when calculated by the numerical approach outlined in Section IV.A. The figure also shows by

This article has been accepted for publication in a future issue of this journal, but has not been fully edited. Content may change prior to final publication. Citation information: DOI 10.1109/TPWRD.2018.2881221, IEEE Transactions on Power Delivery

asterisk the maximum voltage at the tube midpoints as calculated by the respective analytical formulae (19) and (20). It is observed that the analytical formulae give an excellent prediction of the maximum voltages. It is further seen that the induced voltage is lowest (6-9 mV) for the design with a metallic screen inside an insulating layer. When using a cable with metallic screen inside a semiconductive layer, or a semiconductive layer only, the voltage increases to 1-1.5 V and is practically the same for both designs.

Fig. 7 shows the three metallic screen voltages at 50 Hz and the maximum screen voltages as function of frequency, for the design with metallic screen and insulating jacket. The voltages are shown when calculated by the numerical approach described in Section IV.A and by the analytical formula (11). The agreement between the two approaches is excellent up to about 300 Hz but gradually lose accuracy when frequency is further increased.

Fig. 8 shows the maximum voltage along tube 8 when the frequency is varied between 10 Hz and 500 Hz, still assuming operation with 11 kV. The voltage quickly increases with frequency with both designs. The prediction by the analytical formulae (19), (20) is seen to be very good up to about 300 Hz which is above the relevant upper frequency limit for VSD drive applications (pumping and compression). In the kHz range (outside plot range) the agreement becomes very poor as the assumption of constant voltage along the phase conductors is no longer valid, in part due to resonance effects.

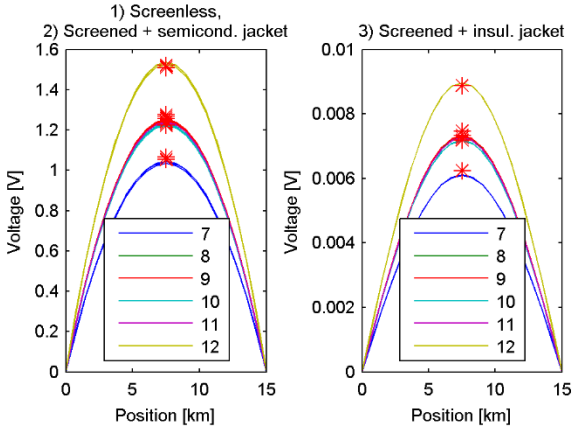

Fig. 6. Tube voltages at 50 Hz. Analytical solution denoted by asterisk.

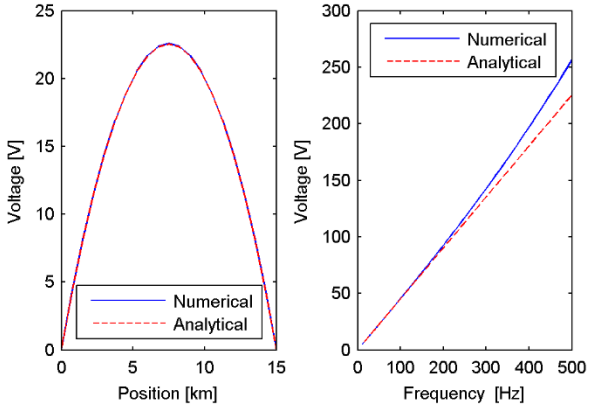

Fig. 7. Screened cables with insulating jacket. Left: screen voltages at 50 Hz along cable; Right: maximum screen voltages as function of frequency.

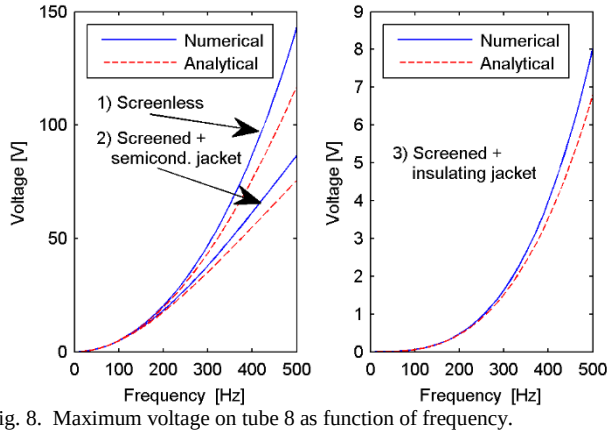

Fig. 8. Maximum voltage on tube 8 as function of frequency.

IX. Puncture Current Density and AC Corrosion Rate

A. Current Density vs. Puncture Radius

We consider that a circular puncture exists on the midpoint in the SD tube with line number 8 in Figs. 4 and 5. The fault impedance Z_{path} is calculated by (35) with Z_{dl}=0, σ=3.3 (sea water), t taken as the tube insulation thickness (1.6 mm), and without any additional impedances representing the inside of the umbilical. As such the calculations are very conservative.

Fig. 9 shows the current density J in the puncture as function of the puncture radius r. It is observed that the current density decreases with increasing puncture radius. The decrease is a result of the voltage on the faulted tube being reduced as the fault current in the water channel increases. The screenless design and the design with a metallic screen plus semiconductive jacket give nearly identical results. With both designs, the theoretically calculated current density at 50 Hz exceeds 1000 A/m^2 when r<2 mm. The 1.6 mm wall thickness is then expected to corrode away in 93 days, according to Table I, if the tube is laid directly in seawater. Although the calculations are conservative, it shows that AC corrosion can be aggressive, potentially causing leakage within a short timeframe.

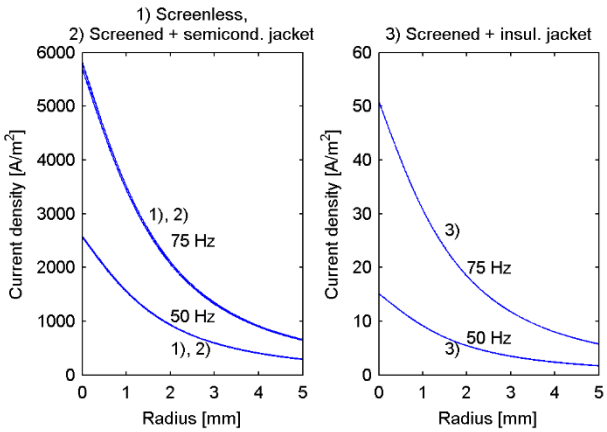

Fig. 9. Current density vs. puncture radius.

B. Current Density vs Cable Length, at 50 Hz.

It was shown in Sections III.A and III.B that the tube voltage is proportional to the second power of length, for the screenless case and for the case with a metallic screen plus an

This article has been accepted for publication in a future issue of this journal, but has not been fully edited. Content may change prior to final publication. Citation information: DOI 10.1109/TPWRD.2018.2881221, IEEE Transactions on Power Delivery

outer semiconductive jacket. Therefore, the current densities will be sufficiently low also for these designs in the case of shorter cables. Fig. 10 shows the current density for a puncture radius of 2.5 mm. It is observed that the current density can be reduced to below a level of 100 A/m^2 by keeping the length below 5 km.

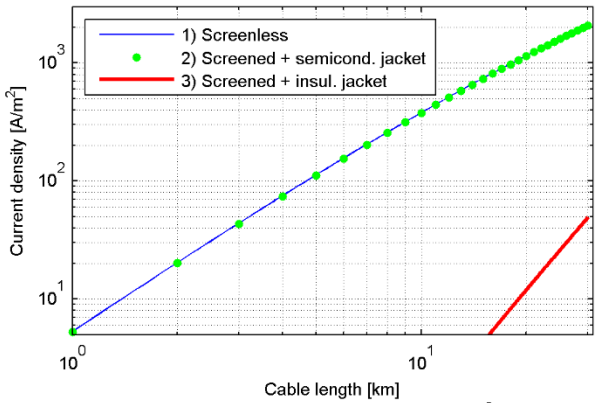

Fig. 10. Current density at 50 Hz vs. cable length, 2.5 mm^2 puncture radius.

X. Tube Voltages in The Presence of Harmonics

The topside VSD converter generates harmonic voltage components which induce additional voltages on the SD tubes. The induced voltages are strongly dependent on the converter filtering, switching frequency and on possible magnification of harmonic voltages by resonance in the power cables.

Using the approach in Section IV.B, the (three) voltage transfer functions from the power cables topside end to the midpoint of tube 8 are calculated under the assumption that the cable is unloaded and fitted [6] with a 20th order rational model as shown in Fig. 11. The voltage response on the tube 8 midpoint is simulated using recursive convolution (31) with applied topside voltages. As an example of voltage application we use reconstructed voltage waveforms from an actual measurement of topside harmonics (in %) in a subsea VSD system operating at 75 Hz. The voltage waveforms are scaled down to give an operating voltage of 6.3 kV line-ground (11 kV line-line), see Fig. 12. Fig. 13 shows the simulated voltage on the midpoint of tube 8, with the three alternative cable designs. The largest oscillation component in Fig. 13 is associated with a 3.6% (227 V line-ground) component at 1275 Hz in the topside voltage which nearly coincides with a peak in the voltage transfer in Fig. 11 for the screenless design. This 1275 Hz component therefore leads to a fairly high voltage on the SD tube (about 180 V peak) while the voltage is lower for the two designs with a metallic screen (45 V peak).

Such high voltages (180 V peak) can be a cause for local heating, as well as severe AC corrosion, if the tube gets exposed to the surrounding seawater in a confined area. To see this effect, we added fault resistance of 51 Ω to tube 8 midpoint that corresponds to a 2.5 mm fault radius by (35). The adding of the fault resistor gave only a modest reduction in the tube voltage. Fig. 14 shows the instantaneous power dissipation associated with the fault resistance. The power dissipation is substantial, being of the order of 100 W.

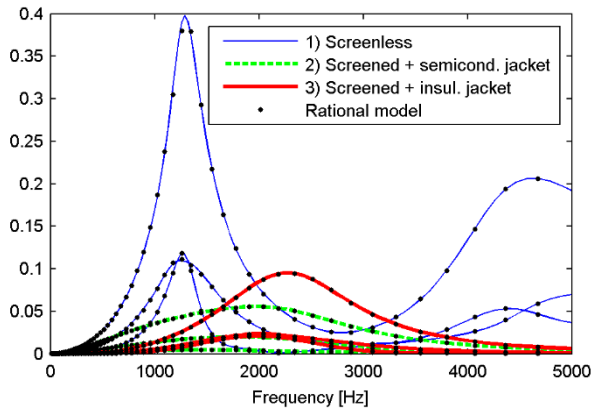

Fig. 11. Voltage transfer from topside cable ends to tube 8 mid-point.

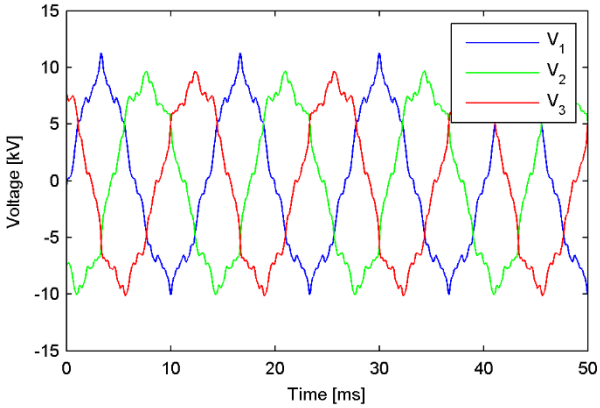

Fig. 12. Topside voltages with operation at 75 Hz.

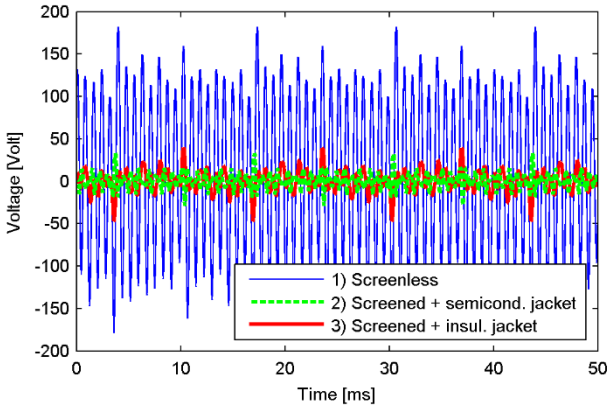

Fig. 13. Calculated voltage on tube 8, at cable mid-point.

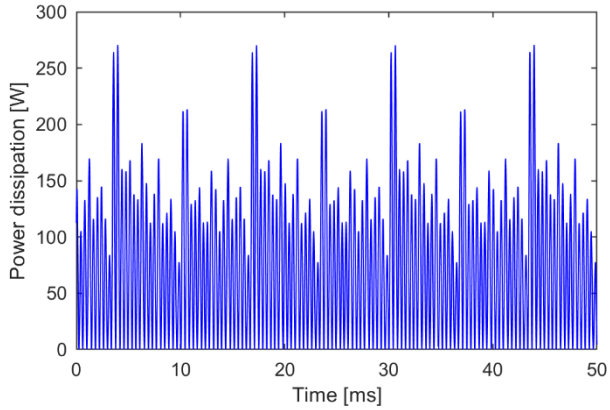

Fig. 14. Calculated power dissipation in a fault puncture of r=2.5 mm added to tube 8 at the cable mid-point.

This article has been accepted for publication in a future issue of this journal, but has not been fully edited. Content may change prior to final publication. Citation information: DOI 10.1109/TPWRD.2018.2881221, IEEE Transactions on Power Delivery

XI. Discussion

The current density in a puncture of the tube coating was shown to decrease with increasing puncture radius, due to a reduction in the tube voltage. For very small puncture radii the corrosion process may stop due to the formation of stationary gas bubbles and corrosion products blocking the channel. Other measurements [13] indicate that bubbles will not form at high pressures (deep waters).

The calculations of current densities were performed under the assumption that the sea water flooding the umbilical represents a zero voltage equipotential. It is likely that this assumption is too conservative, in particular for umbilical designs that utilize extruded filler elements as the space which is occupied by sea water is then quite small. Also, the double layer impedance term Z_{dl} in the channel impedance model (35) was ignored, further overestimating the current density.

It is to be observed that the impedance of the fault reduces the voltage on the tube, thereby also reducing the fault current and associated current density. This effect is included in the calculations by the numerical model in Sections IX and X. However, for small puncture radii (e.g. less than 2 mm), the voltage reduction is quite small. Fig. 15 shows the voltage reduction on tube 8 when introducing a fault on the mid-point with r=5 mm. This plot corresponds to Fig. 6 (left) when there is no puncture.

In the case that the current densities exceed levels where AC corrosion can occur, mitigating steps must be taken. Possible solutions include placement of tubes in a separate twist layer to avoid voltage induction, use of cathodic protection, intermediate grounding of the tubes to reduce voltages, use of bare metal tubes to limit current density, and improved tube coating to reduce risk of punctures. In the case that the induced harmonic voltages are considered the problem, the use a separate twist layers can be used as well as installment of additional harmonic filters.

Three power cable designs were compared regarding the potential risk of AC corrosion on SD tubes. It was shown that design 3), which features a metallic screen and insulating jacket, gave the lowest voltage induction on tubes and thus the lowest risk of AC corrosion. It is however to be observed that with design 3), a voltage results on the metallic screen that the jacket must be able to withstand. This screen voltage increases with the square of the cable length as follows by (11).

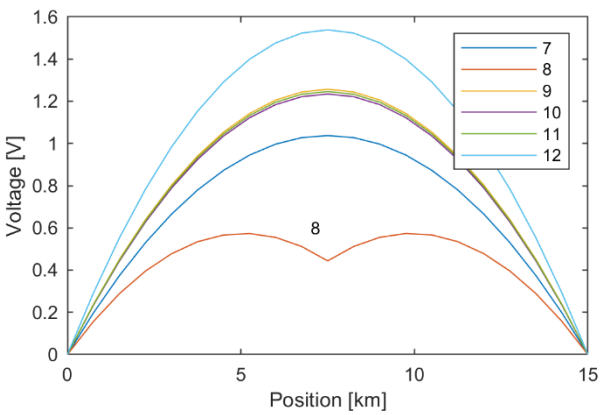

Fig. 15. Calculated tube voltage with a puncture radius of r= 5mm. Screenless cable at 50 Hz.

XII. Conclusion

The longitudinal variation in the flow of charging currents in submarine umbilical power cables gives rise to a non-zero voltage on metallic tubes via magnetic induction, even when they are solidly grounded at both ends. If a puncture exists in the tube coating, AC corrosion can result if the current density becomes sufficiently high.

Measurements were performed on a representative SD tube material, to determine the corrosion rate as function of current density and frequency.

Three alternative designs for the power cables were considered regarding AC corrosion risk: usage of 1) a semiconductive jacket, or 2) a metallic screen inside a semiconductive jacket, or 3) a metallic screen inside an insulating jacket. Calculations show that with operation at 50 Hz, designs 1) and 2) give substantially higher current densities on SD tubes than 3), but the current density decreases quickly when reducing the cable length. Under unfavorable conditions, AC corrosion can lead to puncture of the SD tube in a matter of a few weeks, depending on the umbilical's design and length, and depending on the operation of the electrical system (voltage, frequency).

Additionally, the calculations show that in the presence of harmonic voltage components in the feeding voltage, substantial voltage stresses on the tube coating can result, potentially leading to thermal heating in addition to AC corrosion. The highest voltage were observed for design 1) while designs 2) and 3) gave substantially lower voltages.

The industry should pay attention to the possible risks related to AC corrosion and excessive voltages on the SD tubes. The computational procedures and results presented in this work can be used in practical assessment of alternative solutions and designs.

XIII. Acknowledgement

This project is run by Nexans Norway with SINTEF, NTNU and TechnipFMC as project partners. It is funded by the Research Council of Norway

XIV. References

[1] Offshore Wind Programme Board, "Export Cable Reliability, Description of Concerns", http://www.transmissionexcel.com/wp-content/uploads/2017/07/Export-Cable-Reliability-Step-1-v7-UPDATE-Jul-17.pdf

[2] J. Dabkowski, "Mitigation of Induced Voltages on Buried Pipelines", Material Performance, Vol. 20, No. 1, 1981

[3] Cigré Technical Brochure 95, "Guide on the influence of high voltage ac power systems on metallic pipelines", Working Group 36.02, 1995

[4] M. Pagano, S. Lalvani, "Corrosion of mild steel subjected to alternating voltages in seawater", *Corrosion Science*, vol. 36, pp. 127-140, 1994.

[5] B. Gustavsen, "Validation of frequency dependent transmission line models", *IEEE Trans. Power Delivery*, vol. 20, no. 2, pp. 925-933, April 2005.

[6] B. Gustavsen, and A. Semlyen, "Rational approximation of frequency domain responses by vector fitting", *IEEE Trans. Power Delivery*, vol. 14, no. 3, pp. 1052-1061, July 1999.

[7] M. Büchler, H-G. Schöneich, "Investigation of alternating current corrosion of cathodically protected pipelines: Development of a

detection method, mitigation measures, and a model for the mechanism", *Corrosion*, vol. 65, pp. 578-586, 2009.
[8] J.E.B. Randles, "Kinetics of rapid electrode reactions", Discussions of the Faraday Society, vol. 1, 1947.
[9] British Standard EN 15280:2013, "Evaluation of a.c. corrosion likelihood of buried pipelines applicable to cathodically protected pipelines".
[10] Y-B. Guo, C. Liu, D-G. Wang, S-H. Liu, "Effects of alternating current interference on corrosion of X60 pipeline steel", *Petroleum Science*, vol. 12, pp. 316-324, 2015.
[11] U. Patel, B. Gustavsen, P. Triverio, "Proximity-aware calculation of cable series impedance for systems of solid and hollow conductors", *IEEE Trans. Power Delivery*, vol. 29, no. 5, pp. 2101-2109, October 2014.
[12] B. Gustavsen, M. Høyer-Hansen, P. Triverio, U.R. Patel, "Inclusion of wire twisting effects in cable impedance calculations", *IEEE Trans. Power Delivery*, vol. 31, no. 6, pp. 2520-2529, Dec. 2016.
[13] S. Midttveit and M. Hatlo, "Challenges with combined power and control umbilicals", presentation at Underwater Technology Conf. (UTC), June 12-14, 2017, Bergen, Norway.

XV. BIOGRAPHIES

Bjørn Gustavsen (M'94–SM'2003–F'2014) was born in Norway in 1965. He received the M.Sc. degree and the Dr.Ing. degree in Electrical Engineering from the Norwegian Institute of Technology (NTH) in Trondheim, Norway, in 1989 and 1993, respectively. Since 1994 he has been working at SINTEF Energy Research, currently in the position of Chief Scientist with disciplinary responsibility for the research area of electromagnetic transients.

Martin Høyer-Hansen was born in Norway in 1979. He received the M.Sc. degree in Physics from the Norwegian University of Science and Technology (NTNU) in Trondheim, Norway, in 2003. He currently works as a research scientist at SINTEF Energy Research. His topics of interest include electromagnetic- (EM) and thermal modelling of power cable systems, as well as challenges related to EM interference and AC corrosion.

Marius Hatlo. Was born in Norway in 1980. He received the M.Sc degree in Physics from the Norwegian University of Science and Technology (NTNU) in Trondheim, Norway, in 2005, and PhD from the University of Manchester in 2009. He currently work at Nexans as discipline responsible for the Technological Analysis Centre in Halden. His topics of interest include electromagnetic and thermal modeling of power cable systems, with special emphasis on electromagnetic interference, transient phenomena, harmonics and losses.

Steinar Midttveit was born in Norway in 1962. He graduated from the Norwegian University of Technology in 1985 with a M.Sc. degree in Electrical Power Engineering. Before joining Statoil in 2009, he worked for Framo Engineering for seventeen years. In Framo he worked as a lead engineer within electrical power supply systems for subsea pumping applications, the last period as manager for the Electrical department. During 2009-16 he worked as a Leading Advisor Subsea Electrical Technology, in Statoil. Current position is advisor within subsea electrical power, power cables and power from shore applications.